

Development of an Electrochemical Biosensor for Sulforaphane Determination in Carmine Radish

Xianrong Zhou[#], Bo Jiang[#], Yan Zhang, Jin Shang^{*}, Hui Yang^{*}

College of Life Science and Technology, Yangtze Normal University, Chongqing, 408100, P.R. China

[#]These authors contribute equally

^{*}E-mail: shangjin@yznu.cn; yanghui@yznu.cn

Received: 7 December 2016 / Accepted: 30 December 2016 / Published: 12 February 2017

A multifunctional composite of graphene (Gr), polydopamine (Pdop) and Ag nanoparticles (Ag NPs) was synthesized through a facile and gentle method, where Pdop was immobilized on Gr easily at room temperature and Au NPs was subsequently deposited through gently stirring. The electrochemical responses were investigated at the electrode modified with the composite of Ag, Pdop and Gr by sulforaphane acting as the model molecule. The results indicated that the electrode modified with Ag-Pdop-Gr composite exhibited remarkably favourable for the electron transfer kinetics compared to the glassy carbon electrodes modified with Gr or Ag NPs. At last, the proposed was applied into the simultaneous determination of sulforaphane of trace level in the specimens of carmine radish.

Keywords: Ag nanoparticles; Polydopamine; Graphene; Sulforaphane; Carmine radish

1. INTRODUCTION

Sulforaphane, denoted as [1-isothiocyanate-(4R)-(methylsulfinyl)butane], is a dietetic isothiocyanate. It could be prepared with the precursor existing in the cruciferous vegetables of the species *Brassica* including broccoli, brussels sprouts, cauliflower, cole crops, collards, cress, kale and mustard as well as other category such as radish (*Raphanus* sp.) [1, 2]. Sulforaphane, which is a natural compound, has been extensively researched since 1980s. It has exhibited the chemotherapeutic characteristics such as anti-angiogenic and anti-proliferative properties. Nevertheless, except for anticancer properties, the effects of sulforaphane against the crucial pathologies also has been intensively studied, such as the damage to brain, heart, kidney, liver and muscle as well as hyperglycemia.

Sulforaphane has been demonstrated to exhibit neuroprotective effects in some experimental models. A single ip administration of sulforaphane was reported by Zhao et al. [3] that could decrease the infarct size in rats caused by ischemia as well as reperfusion by the increased expression of HO-1 in brain. A similar protection effect was also observed in an injury model of neonatal hypoxia-ischemia brain, where the levels of 9-hydroxy-2-deoxyguanosine and malondialdehyde were reduced by sulforaphane. Besides, sulforaphane could protect the cells which activate the pathway of Nrf2/ARE, increase the levels of protein and improve the gene transcription as well as the activity of antioxidative enzymes such as γ GCL, HO-1, and NQO1 modifier subunit for the deprivation of glucose and oxygen in astrocytes and immature neurons model [4-6]. Moreover, the blood brain barrier could also be protected by sulforaphane after the brain injury, where the expression of genes driven by Nrf2 was further improved [7]. The cerebral damage, which was caused by the intrastriatal injection of autologous blood, could be prevented by injection of sulforaphane, which also activated Nrf2 in the brain issue influenced by intracerebral haemorrhage (ICH) as well as decreased the oxidative damage, behavioural deficits induced by ICH and neutrophil count [8]. The mice short of Nrf2 exhibited more serious neurologic deficits after ICH and could not be protected by sulforaphane. However, for another brain experiment, inflammation caused by lipopolysaccharide was weakened by the sulforaphane pretreatment combined with Nrf2 induction as well as HO-1 expression in the hippocampus of such brain animals [9]. The mice short of Nrf2 confirmed the role of Nrf2 in this protection effect. The in-vitro researches have been performed to add strength, where sulforaphane was used. The results further confirmed the protection effect of sulforaphane and provided more information on the protection mechanism. For instance, the protection effect of sulforaphane against the oxidation effect of lipopolysaccharide in BV2 microglial cells was in a relation to HO-1 induction. 6-hydroxydopamine as well as tetrahydrobiopterin, which could generate dopamine quinone, could cause the dopaminergic cell death in another cell culture and also could be inhibited by the preincubation of sulforaphane [10]. These results indicated that the pretreatment with sulforaphane could inhibit the formation of reactive oxygen species (ROS), DNA fragmentation and membrane damage. The levels of mRNA as well as the enzymatic activity of NQO1 was increased by sulforaphane in a dose-dependent mode [11]. The rat organotypic and nigrostriatal cocultures could also be protected against the toxicity of 6-hydroxydopamine through introducing Nrf2 secondary to the sulforaphane treatment. The cortical neurons could be protected by sulforaphane from the damage of neurotoxin 5-S-cysteinyl dopamine in another experimental type, as sulforaphane could activate Nrf2 and consequently enhance the expression as well as the activity of GR, glutathione-S-transferase (GST), NQO1 and thioredoxin reductase [12]. Interestingly, sulforaphane increased the time-concentration mode but decreased the levels of GSH in the SH-SY5Y cell line of the dopamine-like neuroblastoma, which was related to the protection effect against 6-hydroxydopamine or H_2O_2 [13].

However, the electrochemical performance of sulforaphane has only been investigated by Fijalek and co-workers by far [14], where the voltammetric approaches was based on oxidizing the isothiocyanate group with a cathodic peak E_p of -0.6 V. The current results have been statistically evaluated, indicating that a satisfactory accuracy and precision (1.60% R.S.D) is obtained towards the determination of SFR with the developed processes. UV spectrophotometry was employed to assess the stability of the analysed solution. The CV approach combined with gold electrode could be applied

into the determination and identification of this compound, taking in account of the desirable rapidity, selectivity, sensitivity and the ease to carry out determinations.

Due to the distinct chemical and physical properties including outstanding stability, high surface area, strong mechanical strength and remarkable electrical conductivity, graphene (Gr) has attracted intensive interest of researchers [15]. Hence, Gr has become a promising candidate for the fabrication of diverse functional devices including electrodes, photodetectors, photovoltaics and sensors [16, 17]. Ag NPs have been demonstrated to exhibit excellent conductivity and remarkable electrochemically catalytic activity. Besides, the possibilities to prepare Ag-doped nanomaterials as well as the application in biosensor could be expanded by the availability of Ag NPs [18]. The combination of metal nanoparticles with carbon-based materials have been reported to display synergistic effects on the electro-catalytic applications [19]. Consequently, the integration of Ag NPs and Gr is supposed to obtain a similar effect on electro-oxidizing adenine and guanine.

Polydopamine (Pdop) layer, which is a thin, multifunctional and surface adherent biopolymer, have been produced recently through the self-polymerization of dopamine in aqueous solution on diverse organic and inorganic materials [20-25]. Various ad-layers have been generated through the Pdop coating, such as bioactive surfaces by macromolecules graft, metal films through metallization without electroplating and self-assembled monolayer through the deposition of blocks built with long-chain molecular [26]. The polymerization of dopamine, which exhibits the superiority of surface functionalization in single step, could introduce a new paradigm into the surface modification area. Herein, a novel multifunctional composite of Ag NPs, Pdop and Gr was synthesized via oxidizing dopamine on Gr and the subsequent electrodeposition of silver under mildly stirring. An improved catalytic performance was observed with the GCE modified by AgNPs-Pdop@Gr to determine sulforaphane. Additionally, the fabricated biosensor was also employed into the determination of sulforaphane in the specimens of carmine radish successfully.

2. EXPERIMENTS

2.1. Chemicals

Sulforaphane (98%) was prepared in the Laboratory of Physicochemical Principles of Chemical Technology of Zhejiang University, and then was purified through distilling twice when the pressure was 0.01 mm Hg. Ammonia solution (28 wt%), graphite powder and hydrazine solution (50 wt%) were commercially available in Shanghai Chemical Reagent Corporation (Shanghai, China). 2-amino-2-hydroxymethylpropane-1,3-diol (Tris), adenine, dopamine hydrochloride (DA) and guanine were purchased in Sigma (Saint Louis, MO, USA). Besides, acetate buffer solutions (ABS) were produced through mixing CH₃COOH and CH₃COONa (0.1 M), where the pH was adjusted with NaOH. All the chemicals were analytically pure. Besides, the doubly distilled water was employed throughout all the experiments.

2.2. Apparatus

A CHI 660D electrochemical workstation (Shanghai CH Instruments, China) was employed to conduct electrochemical measurements through combining the three-electrode system in all the experiments. A bare GCE, a pretreated GCE as well as a GCE modified with AgNPs-Pdop-Gr composite, which were all with a diameter of 3 mm, were employed as the working electrode. Besides, a platinum wire as well as a saturated calomel electrode (SCE) were utilized as the auxiliary electrode and reference electrode, respectively. Autolab Electrochemical Instruments (Autolab, Eco Chemie, The Netherlands) was used to perform the electrochemical impedance spectroscopy in the mixture of $K_3Fe(CN)_6/K_4Fe(CN)_6$ in a ratio of 1:1 (5.0 mM) containing KCl (0.1 M) acting as the support electrolyte, where the voltage of alternating current was 5 mV and the frequency range was 0.1 to 10^5 Hz. Scanning electron microscope (SEM, Hitachi S-4800) was utilized to investigate the morphologies of the nanocomposite.

2.3. Preparation of AgNPs-Pdop-Gr nanocomposite

The modified Hummers method was employed to prepare graphene oxide (GO) with graphite powder [27]. According to the typical procedure, graphite (5 g) was added into the mixture of the fuming HNO_3 (45 mL) and the concentrated H_2SO_4 (87.5 mL). Noted that the fuming HNO_3 and the concentrated H_2SO_4 are strong oxidants and need to be carefully handled. Then, $KClO_3$ (55 g) was added into the formed mixture and stirred for 96 h. Subsequently, the generated slurry was added into water and filtered to gain the graphite oxide. After being dried at 80 °C, the graphite oxide (0.5 g) was exfoliated through ultrasonic in 500 mL to generate the colloidal suspension of graphene oxide with a concentration of 1 mg/mL. The GO suspension was then reduced by hydrazine monohydrate at 80 °C for 24 h to produce Gr. Then, the obtained product was filtered and washed with pure water and ethanol completely. At last, the target product was dried to obtain Gr under vacuum.

The nanocomposite of Ag NPs, Pdop and Gr was synthesized according to the procedures described below. First, Gr (100 mg) was dispersed into water (100 mL) through sonication. Then, DA (200 mg) and Tris (120 mg) were added into the obtained mixture and sonicated again for 1 min with ice water bath. After being stirred for 20 h at room temperature, the as-prepared product was filtered, rinsed and dried at 60 °C overnight under vacuum to gain Pdop-Gr. Thereafter, the mild deposition of Ag NPs was performed on the Pdop-Gr surface, where Pdop-Gr (25 mg) was added into the aqueous solution of $AgNO_3$ (25 mL). Subsequently, the mixture was gently stirred at room temperature for 2 h. At last, the nanocomposite of AuNPs, Pdop and Gr was obtained after the successive filtration, washing and drying of the generated product overnight at 60 °C under vacuum.

3. RESULTS AND DISCUSSION

The adhesive Pdop was reported to be formed through the self-polymerization of dopamine under a weak basic condition [28]. In this work, this approach was employed to modify the GO sheets

with Pdop. First, FTIR spectroscopy was used to characterize the modified GO sheets. In Figure 1A, the peaks in the IR spectrum of GO located at 1730, 1620, 1398 and 1047 cm^{-1} , which were attributed to the C=O stretching of COOH groups, the C=O stretching vibration, the C—OH stretching vibration as well as C—O vibrations of alkoxy groups, respectively. However, the intensity of these peaks decreased significantly when Pdop was functionalized on GO, which indicated that the content of the oxygen-based groups remarkably decreased on the GO surface. This might be due to the chemical reduction of oxygen groups on the GO surface with dopamine during the process of self-polymerization, where dopamine and its derivatives could serve as the reductants [11]. Hence, the GO sheets functionalized with Pdop was defined as Pdop-Gr. Moreover, two new peaks at 1503 and 1358 cm^{-1} were also observed with the sample of Pdop-Gr, which were ascribed to the stretching vibration of C=N as well as C-N-C of indole ring, respectively. This indicated that Pdop was successfully deposited on the GO sheets. Though the absorbance of the whole visible range has a big increase, the dispersion of PDA-RGO does not show any perceptible precipitation, implying that the formed PDA is a great stabilizer to prevent the stacking of the reduced graphene sheets.

XRD was employed to analyse the crystal structure of GO as well as the Pdop-Gr/Ag composite. In Figure 1C, a representative characteristic peak (001) located at 11.1° was observed with GO, whereas this peak did not present in PDA-RGO/Ag composite. This result indicated that GO was reduced after being modified with PDA. The diffraction peak (003) located at 28° was assigned to the regional RGO sheets, which restacked into the well-organized crystalline structure [13]. Besides, the rest diffraction peaks present at 80.1° , 77.7° , 64.8° , 44.4° and 38.1° were attributed to the (222), (311), (220), (200) and (111) planes of the Ag NPs, respectively.

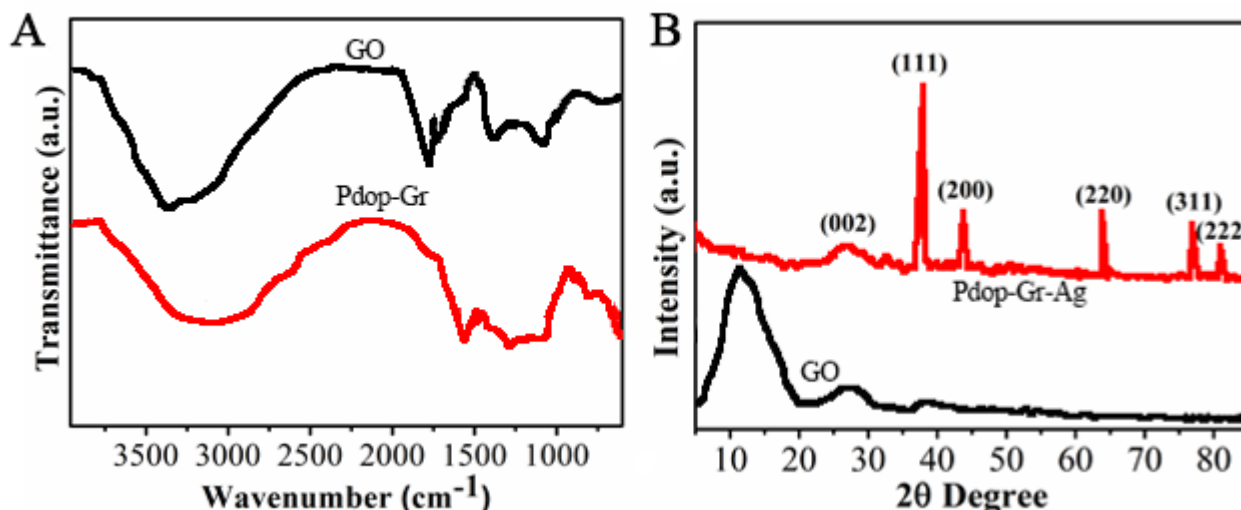


Figure 1. (A) FTIR spectra of GO and Pdop-Gr. (B) XRD patterns of GO and Pdop-Gr/Ag.

SEM was employed to investigate the morphology of the composite of Pdop-Gr/Ag, where the recorded SEM images were depicted in Figure 2. Compared to the original GO sheets shown in Figure 2A, the Pdop-Gr/Ag composite illustrated in Figure 2B exhibited a homogenous deposition of Ag NPs

on the surface of Gr sheets functionalized with Pdop. In Figure 2C, the mean size of Ag NPs was calculated to be 100 nm through counting more than 200 Ag NPs and fitting the size distribution with the Gaussian function. Figure 2D showed the elements information of the Pdop-Gr/Ag composite measured through EDX, where only C, N, O and Ag were found in the spectrum. The spectrum presents the only existence of C, N, O and Ag, indicating the successful formation of the composite with high purity [21].

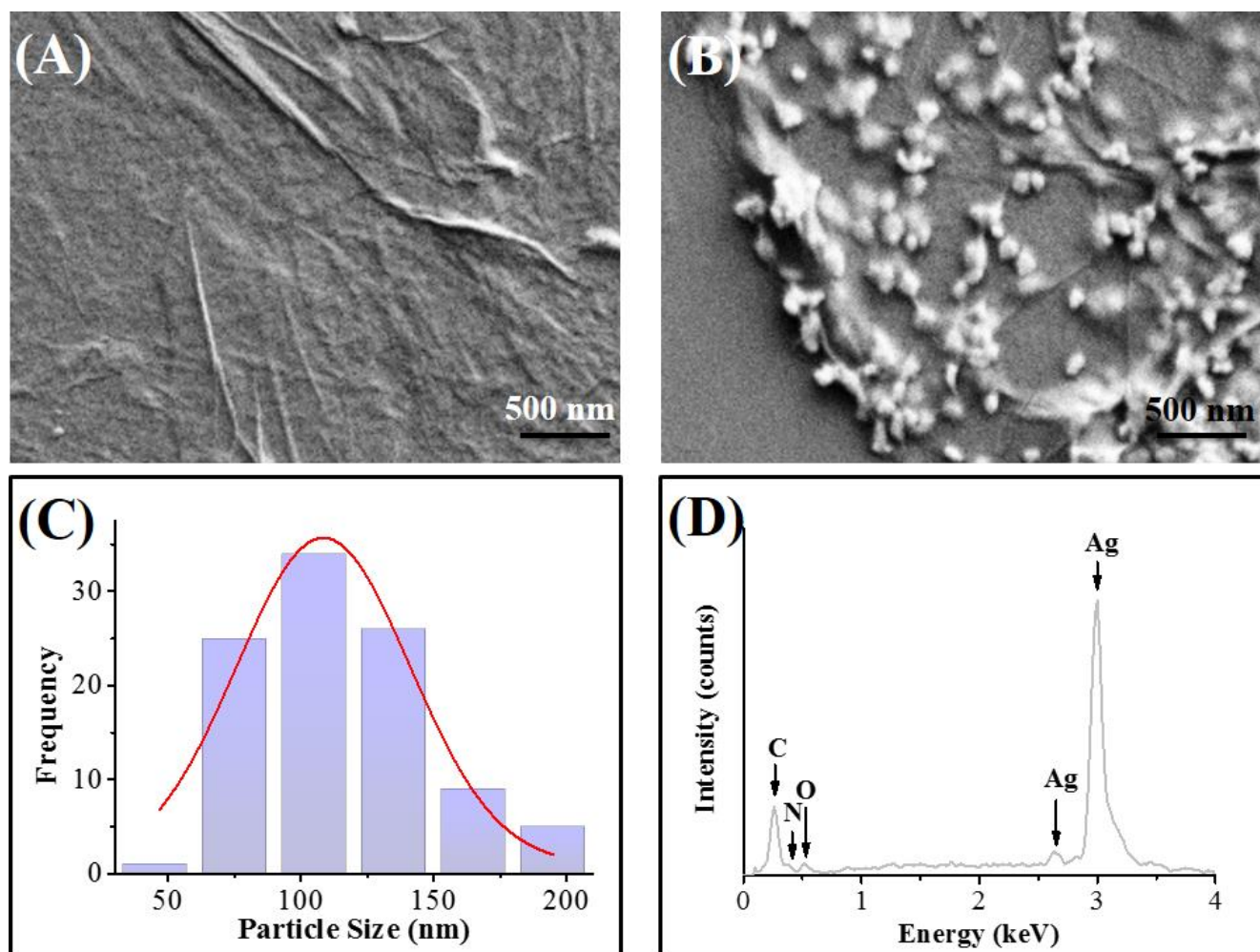


Figure 2. SEM images of (A) GO, (B) Pdop-Gr/Ag. (C) Size distribution of Ag nanoparticles. (D) EDX spectrum of Pdop-Gr/Ag.

AC impedance experiments were carried out to investigate the electron transfer performance of various electrodes, where the results were illustrated in Figure 3A. It was obvious that the order of the resistance values of charge transfer of diverse electrodes was $GCE < AgNPs/GCE < Gr/GCE < AgNPs-Pdop-Gr/GCE$. It indicated that AgNPs-Pdop-Gr/GCE exhibited higher electrochemical capacity compared with the other electrodes. The electron transfer resistance (R_{ct}) was measured to be 545 Ω , 655 Ω , 684 Ω and 777 Ω at the bare AgNPs-Pdop-Gr/GCE, Gr/GCE, AgNPs/GCE and GCE respectively, after the optimization of the equivalent and calculation. A significant increase of R_{ct} was

observed when depositing AgNPs-Pdop-Gr/GCE surface. Moreover, the analytical applications were significantly influenced by the potential window of these electrodes. As shown in Figure 3B, the potential window of AgNPs-Pdop-Gr/GCE in ABS (0.1 M) with a pH of 4.0 was around 2.75 V, which was approximate to that of the bare GCE as well as Gr/GCE but higher compared to that of AgNPs/GCE.

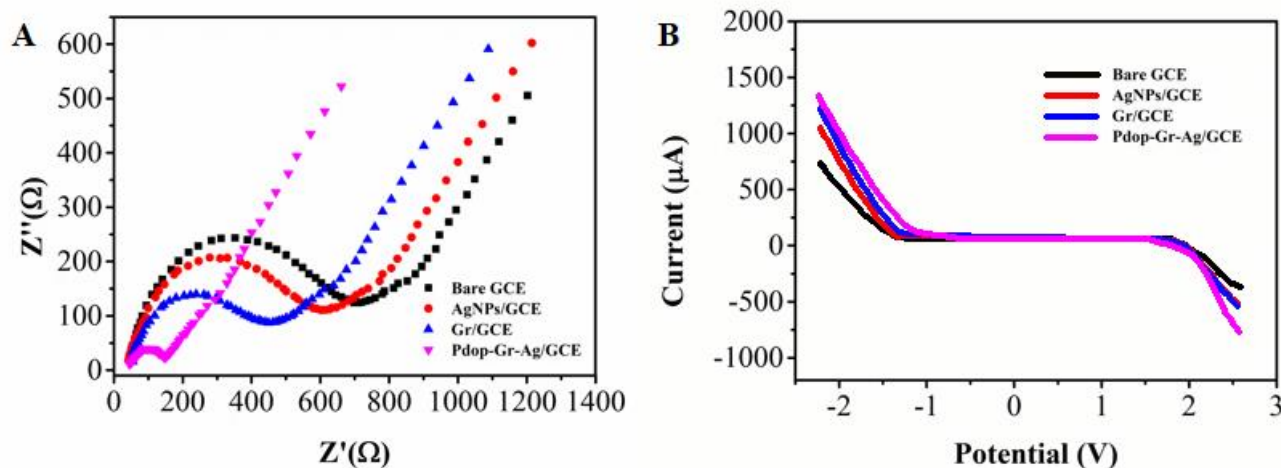


Figure 3. (A) Nyquist plots obtained at GCE, AgNPs/GCE, Gr/GCE and AgNPs-Pdop-Gr/GCE in $\text{Fe}(\text{CN})_6^{3-/4-}$ (5 mM) with KCl (0.1 M) with a frequency range of 0.1 Hz to 10 kHz. (B) LSVs of GCE, AgNPs/GCE, Gr/GCE and AgNPs-Pdop-Gr/GCE in PBS (0.1 M) with a pH of 7.0. Scan rate: 50 mV/s.

The chronocoulometric curves of the reduction of $\text{K}_3\text{Fe}(\text{CN})_6$ (1mM) with KCl (2 M) obtained at various electrodes was shown in Figure 4A. The equation was described below:

$$Q = (2nFAD_0^{1/2} / 2\pi^{-1/2} C_0) t^{1/2}$$

The absolute value of the reduction charge was Q , where n represented the number of electrons in this reaction. The diffusion coefficient of the oxidation state of hexacyanoferrate (III), the apparent area of electrode as well as the Faraday constant were depicted with D_0 , A and F , respectively. Besides, C_0 clarified the bulk concentration of the oxidation state while t represented the time. According to the slope of the $Q-t^{1/2}$ line, the order of A of various electrodes was calculated to be $\text{GCE} < \text{AgNPs/GCE} < \text{Gr/GCE} < \text{AgNPs-Pdop-Gr/GCE}$. This results indicated that AgNPs-Pdop-Gr/GCE might exhibit the greatest electrochemical performance among them as it obtained the maximum value of A .

Figure 4B showed the electrochemical response of the electrodes with $\text{Fe}(\text{CN})_6^{3-/4-}$ after diverse modifications. On the carbon electrodes, $\text{Fe}(\text{CN})_6^{3-/4-}$ was approximate to the ideal quasi-reversible system. The maximum peak current was obtained with AgNPs-Pdop-Gr/GCE, indicating that the definite AgNPs-Pdop-Gr exhibited the necessary surface structure as well as electronic capacities to provide quick electron transfer for such extraordinary and mechanistically sophisticated redox system. It is expected the AgNPs-Pdop-Gr could exhibit an advanced performance towards electrochemical sensor application.

Figure 5A clarified the CV profiles of the oxidation of sulforaphane in PBS (1 mM), which were recorded at the bare GCE, Gr/GCE as well as AgNPs-Pdop-Gr/GCE. A significantly low current was obtained with the bare GCE under a potential of 0.79 V, suggesting that the oxidation of sulforaphane was remarkably weak at the bare GCE electrode. On the contrary, the observed current response was considerably high at Gr/GCE and even much higher at AgNPs-Pdop-Gr/GCE. No peak response was observed in the absence of sulforaphane, which confirmed that the peak was ascribed to the oxidation of sulforaphane at potential of 0.67 V. Moreover, the shifting potential of the oxidation peak demonstrated that the over-potential of the oxidation of sulforaphane became lower as the AgNPs-Pdop-Gr nanocomposite exhibited an electrocatalytic activity.

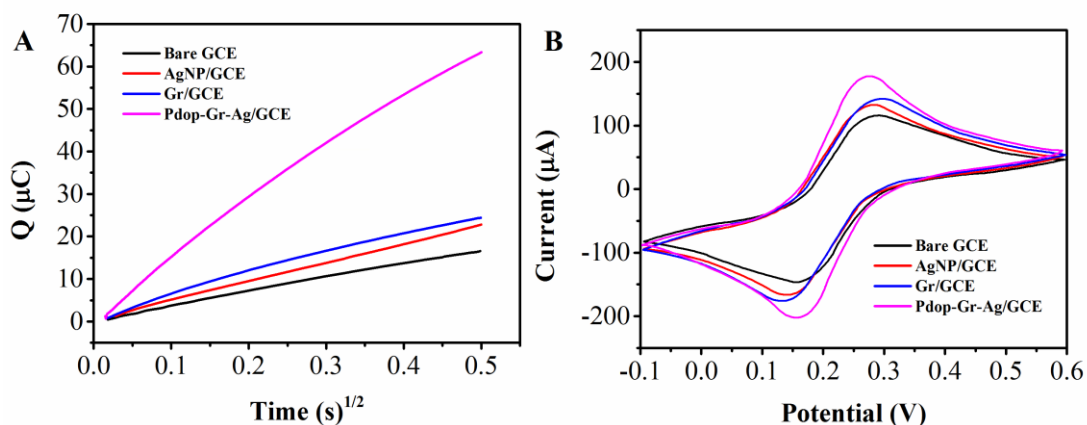


Figure 4. (A) Chronocoulometric curves of the reduction of $K_3Fe(CN)_6$ (1mM) at GCE, AgNPs/GCE, Gr/GCE as well as AgNPs-Pdop-Gr/GCE in the presence of KCl (2M), where the potential was varied from 0.65 to -0.05 V. (B) CVs of GCE, AgNPs/GCE, Gr/GCE as well as AgNPs-Pdop-Gr/GCE in $Fe(CN)_6^{3-/4-}$ (5 mM) with KCl (0.1 M).

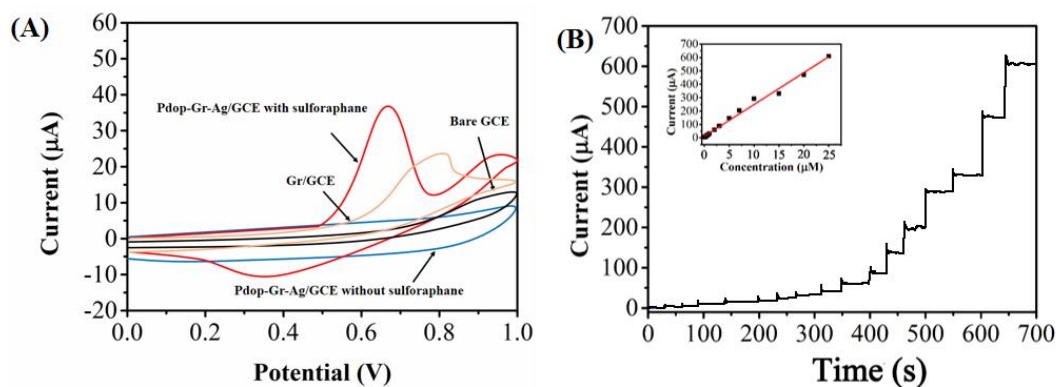


Figure 5. (A) CVs of the oxidation of sulforaphane at the bare GCE, Gr/GCE as well as AgNPs-Pdop-Gr/GCE. Scan rate: 50 mV/s. (B) The relationship the amperometric response obtained at AgNPs-Pdop-Gr/GCE with a potential of 0.67 and the successive addition of sulforaphane into PBS. Inset was the magnification of the current responses with a concentration ranging from 0.05 to 25 μM.

Figure 5B illustrated the relationship between the amperometric response of AgNPs-Pdop-Gr and the continuous addition of sulforaphane. After adding sulforaphane, the response would reach the steady state in 4 s, which indicated that AgNPs-Pdop-Gr exhibited a remarkably fast detection performance. In Figure 5B, the current responses displayed a linear relationship with the concentration of sulforaphane in the range of 0.05 to 50 μM . The limit of detection was measured to be 10 nM when the ratio of signal to noise was 3. The sensitivity of the proposed sensor was compared with that of other reported sulforaphane sensors and the results were presented in Table 1.

Table 1. Comparison of the present electrochemical sensor with other sulforaphane determination methods.

Method	Linear detection range	Detection limit	Reference
HPLC	—	3 $\mu\text{g/g}$	[29]
GC-MS	—	—	[30]
LC-MS/MS	0.01–0.1 μM	—	[31]
AgNPs-Pdop-Gr/GCE	0.05 to 50 μM	10 nM	This work

Furthermore, the analysis of sulforaphane of trace level in the specimen of carmine radish was performed with the biosensor, which was fabricated with AgNPs-Pdop-Gr/GCE. Two samples of carmine radish, which were commercially available in local market, was used as the practical samples. In Table 2, the detected concentration of sulforaphane in the two commercial samples indicated that the electrochemical sensor fabricated with AgNPs-Pdop-Gr/GCE exhibited outstanding capacity towards the detection of sulforaphane in the vegetable specimens. Thus, the constructed electrochemical sensor were potential in the practical determination of sulforaphane in diverse food specimens.

Table 2. Determination of sulforaphane in the specimens of carmine radish through the electrochemical sensor based on AgNPs-Pdop-Gr/GCE.

Sample	Added (μM)	Found (μM)	Recovery (%)
Carmine radish 1	0	1.24	—
	2	3.44	106.12
	5	6.35	101.76
	10	11.52	102.49
Carmine radish 2	0	1.59	—
	0.5	2.04	78.76
	3	4.66	101.53
	6	7.43	97.89

4. CONCLUSIONS

In conclusion, a new electrochemical sensor was constructed with the GCE modified by the composite of Ag NPs, Pdop and Gr to determine sulforaphane sensitively. The nanocomposite of

AgNPs-Pdop-Gr was synthesized through a facile approach, where dopamine was oxidized on the surface of Gr at room temperature and Ag was subsequently electrodeposited under mildly stirring. The electron transfer between the underlying electrode and the analytes was remarkably enhanced by the nanocomposite of AgNPs-Pdop-Gr. The linear range as well as the limitation of detection was measured to be 0.05 to 50 μ M and 10 nM, respectively. In addition, the as-prepared electrochemical sensor could also be applied into the determination of carbendazim in the practical specimens of carmine radish.

ACKNOWLEDGEMENT

This research was supported by the National Natural Science Foundation of China(31470568), the Scientific and Technological Project of Chongqing(cstc2015jcyjA80002), the Key Laboratory of Protection and Utilization of Wulingshan Region's Unique Plant Resources of Chongqing(2016)

References

1. J.W. Fahey, A.T. Zalcman and P. Talalay, *Phytochemistry*, 56 (2001) 5.
2. G. van Poppel, D.T. Verhoeven, H. Verhagen and R.A. Goldbohm, Brassica vegetables and cancer prevention, *Advances in Nutrition and Cancer 2*, Springer1999, pp. 159.
3. J. Zhao, N. Kobori, J. Aronowski and P.K. Dash, *Neuroscience letters*, 393 (2006) 108.
4. Z. Ping, W. Liu, Z. Kang, J. Cai, Q. Wang, N. Cheng, S. Wang, S. Wang, J.H. Zhang and X. Sun, *Brain research*, 1343 (2010) 178.
5. L. Soane, W. Li Dai, G. Fiskum and L.L. Bambrick, *Journal of neuroscience research*, 88 (2010) 1355.
6. C.A. Danilov, K. Chandrasekaran, J. Racz, L. Soane, C. Zielke and G. Fiskum, *Glia*, 57 (2009) 645.
7. J. Zhao, A.N. Moore, J.B. Redell and P.K. Dash, *The Journal of Neuroscience*, 27 (2007) 10240.
8. X. Zhao, G. Sun, J. Zhang, R. Strong, P.K. Dash, Y.W. Kan, J.C. Grotta and J. Aronowski, *Stroke*, 38 (2007) 3280.
9. N.G. Innamorato, A.I. Rojo, Á.J. García-Yagüe, M. Yamamoto, M.L. De Ceballos and A. Cuadrado, *The Journal of Immunology*, 181 (2008) 680.
10. J.M. Han, Y.J. Lee, S.Y. Lee, E.M. Kim, Y. Moon, H.W. Kim and O. Hwang, *Journal of Pharmacology and Experimental Therapeutics*, 321 (2007) 249.
11. A. Siebert, V. Desai, K. Chandrasekaran, G. Fiskum and M.S. Jafri, *Journal of neuroscience research*, 87 (2009) 1659.
12. D. Vauzour, M. Buonfiglio, G. Corona, J. Chirafisi, K. Vafeiadou, C. Angeloni, S. Hrelia, P. Hrelia and J.P. Spencer, *Molecular nutrition & food research*, 54 (2010) 532.
13. A. Tarozzi, F. Morroni, A. Merlicco, S. Hrelia, C. Angeloni, G. Cantelli-Forti and P. Hrelia, *Journal of neurochemistry*, 111 (2009) 1161.
14. Z. Fijałek, K. Sarna and T. Kasprzycka-Guttman, *Journal of Pharmaceutical and Biomedical Analysis*, 32 (2003) 967.
15. H. Wang, T. Chen, S. Wu, X. Chu and R. Yu, *Biosensors and Bioelectronics*, 34 (2012) 88.
16. M. Zhou, Y. Zhai and S. Dong, *Anal. Chem.*, 81 (2009) 5603.
17. C. Yang, Y. Chai, R. Yuan, W. Xu, T. Zhang and F. Jia, *Talanta*, 97 (2012) 406.
18. H. Chen, D. Tang, B. Zhang, B. Liu, Y. Cui and G. Chen, *Talanta*, 91 (2012) 95.
19. Q. Zhang, Q. Ren, Y. Miao, J. Yuan, K. Wang, F. Li, D. Han and L. Niu, *Talanta*, 89 (2012) 391.
20. H. Lee, S.M. Dellatore, W.M. Miller and P.B. Messersmith, *science*, 318 (2007) 426.
21. L. Fu, G. Lai, B. Jia and A. Yu, *Electrocatalysis*, 6 (2015) 72.
22. L. Fu, G. Lai, D. Zhu, B. Jia, F. Malherbe and A. Yu, *ChemCatChem*, 8 (2016) 2975.
23. L. Fu and A. Yu, *Nanoscience and Nanotechnology Letters*, 7 (2015) 147.

24. D. Hafner, L. Ziegler, M. Ichwan, T. Zhang, M. Schneider, M. Schiffmann, C. Thomas, K. Hinrichs, R. Jordan and I. Amin, *Adv. Mater.*, 28 (2016) 1330.
25. Y. Song, G. Ye, F. Wu, Z. Wang, S. Liu, M. Kopeć, Z. Wang, J. Chen, J. Wang and K. Matyjaszewski, *Chemistry of Materials*, 28 (2016) 5013.
26. C.L. Randall, E. Gultepe and D.H. Gracias, *Trends in biotechnology*, 30 (2012) 138.
27. W.S. Hummers Jr and R.E. Offeman, *Journal of the American Chemical Society*, 80 (1958) 1339.
28. M.H. Ryou, Y.M. Lee, J.K. Park and J.W. Choi, *Adv. Mater.*, 23 (2011) 3066.
29. H. Liang, Q.P. Yuan, H.R. Dong and Y.M. Liu, *Journal of Food Composition and Analysis*, 19 (2006) 473.
30. W.C. Chiang, D.J. Pusateri and R.E. Leitz, *Journal of Agricultural and Food Chemistry*, 46 (1998) 1018.
31. S. Agrawal, B. Winnik, B. Buckley, L. Mi, F.-L. Chung and T.J. Cook, *Journal of Chromatography B*, 840 (2006) 99.

© 2017 The Authors. Published by ESG (www.electrochemsci.org). This article is an open access article distributed under the terms and conditions of the Creative Commons Attribution license (<http://creativecommons.org/licenses/by/4.0/>).